Electronic Supplementary Information (EIS)

Constructing epitaxial grown heterointerface of metal nanoparticles and manganese dioxide anode for high-capacity and high-rate lithium-ion batteries

Jianwei Zhang[a,#], Danyang Huang[a,#], Yuchen Wang[a], Liang Chang[a], Yanying Yu[a], Fan Li[a], Jia He[a], Dongqi Liu[b,] and Chao Li[a,*]*

[a]Center for Electron Microscopy and Tianjin Key Lab of Advanced Functional Porous Materials, Institute for New Energy Materials and Low-Carbon Technologies, School of Materials Science and Engineering, Tianjin University of Technology, Tianjin 300384, China.

[b]School of Physics, Nankai University, Tianjin 300071, China.

E-mail: chao_li@tjut.edu.cn, liudq@nankai.edu.cn

Figures and Tables

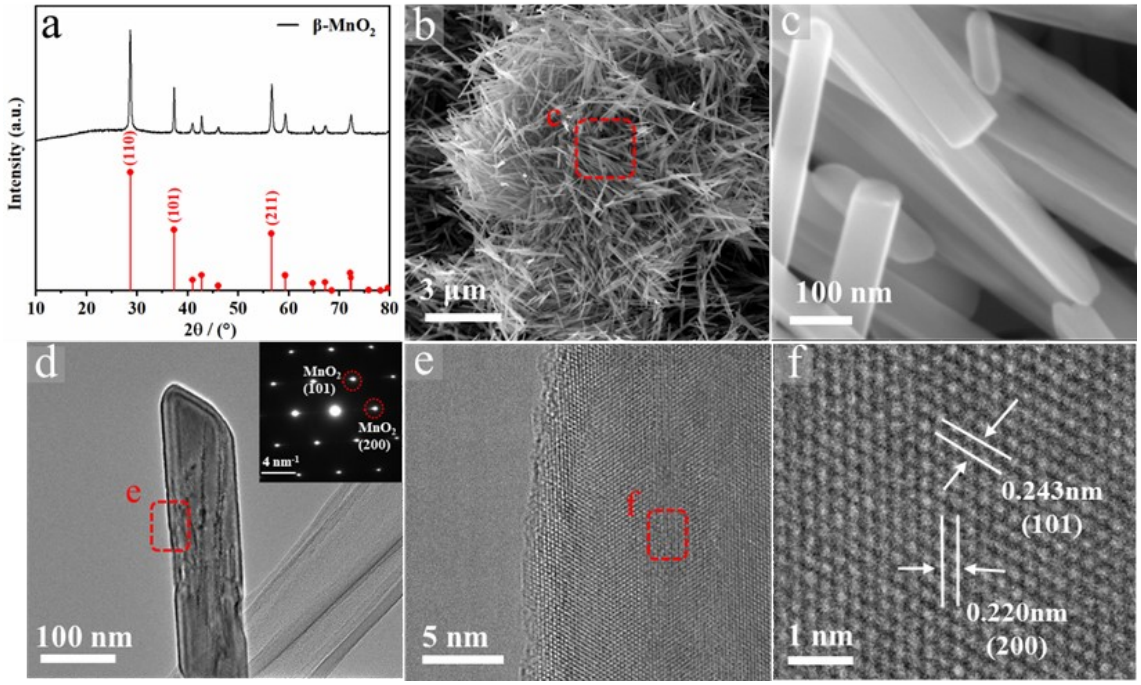

Figure S1. (a) X-ray diffraction pattern (b) low- and (c) high-magnification SEM images (d) HRTEM image and SAED pattern (inset) (e) low- and (f) high-magnification HRTEM images of MnO_2.

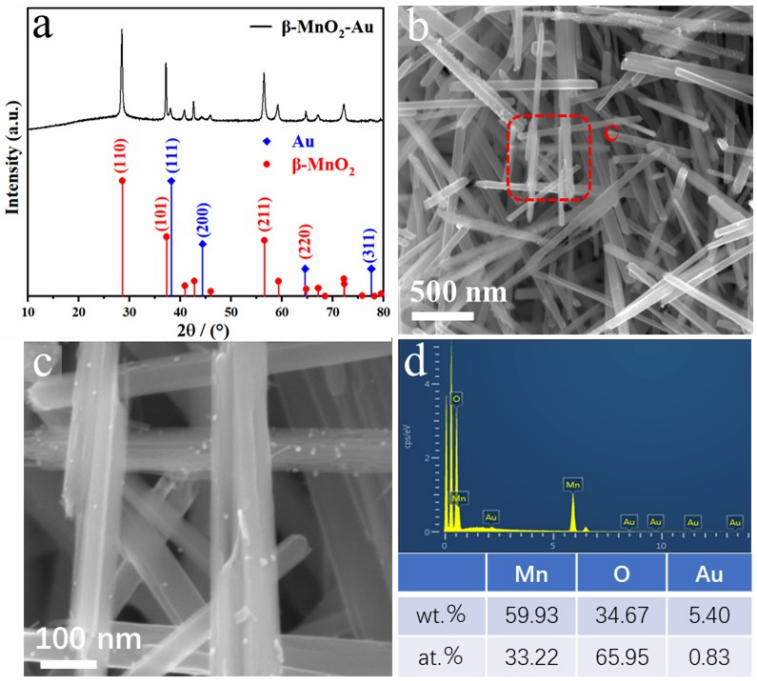

Figure S2. (a) X-ray diffraction pattern (b) low- and (c) high-magnification SEM images (d) Elemental analysis and a table for atomic and mass percentages of Mn, O and Au of MnO_2-Au heterostructure nanorods.

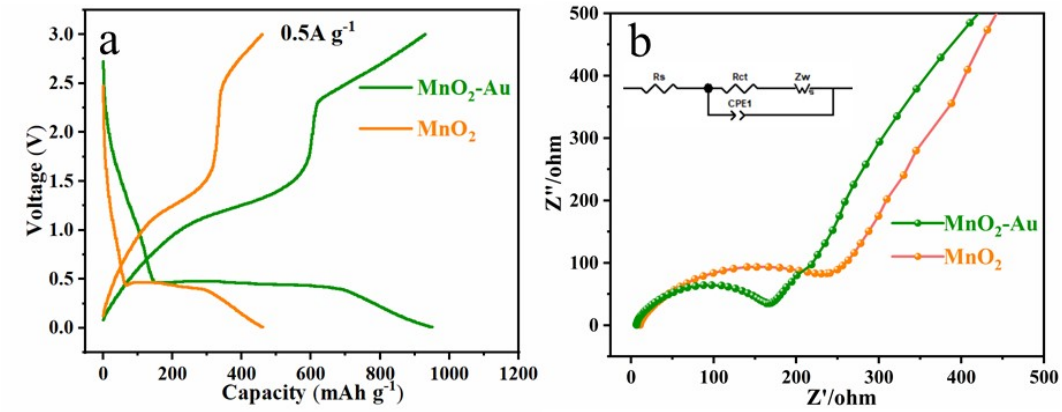

Figure S3. (a) The typical charge-discharge profiles of MnO_2 and MnO_2-Au at current density of 500 mA g^{-1} (b) The Nyquist plots of the impedance spectra of cells of MnO_2 and MnO_2-Au. The equivalent circuit model is exhibited in the insert of Fig. S3(b). The intercept of the high-frequency semicircle on the *Z'* axis can be attributed to the resistance of the electrolyte (R_s). R_{ct} are charge transfers resistance. The fitting values of kinetic parameters of MnO_2 and MnO_2-Au cells are shown in Table S1. Compared with MnO_2, MnO_2-Au shows lower R_{ct}, which indicates that MnO_2-Au heterojunction promotes the diffusion of lithium ions and electrons at the electrolyte/electrode interface.

Table S1 Kinetic parameters of the MnO_2-Au and MnO_2 electrode.

	$R_s(\Omega)$	$R_{ct}(\Omega)$
MnO_2-Au	6.10	163.3
MnO_2	10.11	234.5

Table S2 Summary Comparison of Electrochemical Performance between MnO_2-Au and Other Manganese Oxide-Based Materials for LIBs

Materials	Cycle numbers	Current density (mA g^{-1})	Specific capacity (mA h g^{-1})	ref
MnO_2-Au		50/100/300	1250.6/1211.8/1067.1	This work
	130	1000	942.3	
MnO_2-TiO_2-Carbon	130	100	677	1
Co_3O_4/MnO_2/C	100	200	854.9	2
MnO_2–PEI–RGO	50	100	880	3
MnO2@C Foam	50	100	840	4
G-CNT-Fe	45	100	1024	5
MnO_2-MoO_3	50	100	1000	6
MnO@mcarbon	60	100	872.8	7

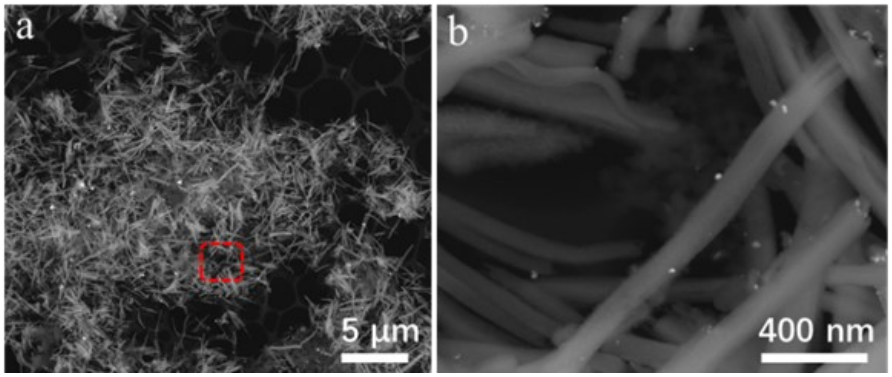

Figure S4 (a) low- and (b) high-magnification BSE images of MnO_2-Au electrode at 60th with a current density of 1 A g^{-1}. The low-magnification SEM image shows that MnO_2 preserves the shape of the nanorod during the cycle process. The size of Au nanoparticles is about 20 nm, which is larger than the original size of Au nanoparticles (~5-10 nm). This result indicates that Au nanoparticles have some degree of agglomeration during the charging and discharging process.

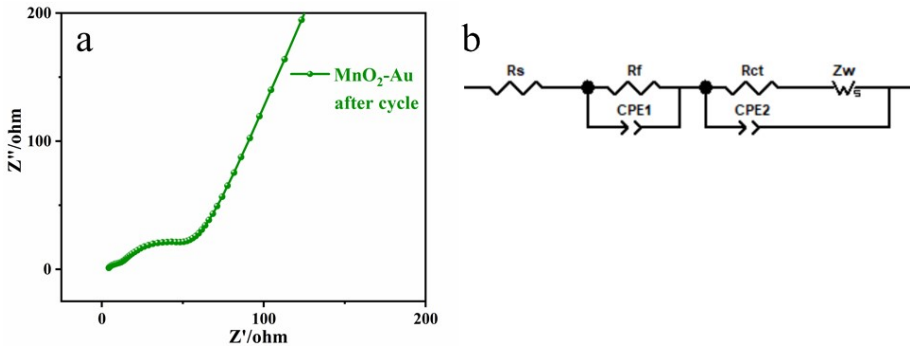

Figure S5. (a) The Nyquist plots of the impedance spectra of MnO_2-Au cells at 60th with a current density of 1 A g^{-1} (b) The equivalent circuit of the Nyquist plot. The equivalent circuit used for fitting is show in Fig. S5 (b), where (R_f) is the resistance of SEI film. After circulation, R_s and R_{ct} of MnO_2-Au decreased.

Table S3 Kinetic parameters of the MnO_2-Au electrode after cycle.

	$R_s(\Omega)$	$R_f(\Omega)$	$R_{ct}(\Omega)$
MnO_2-Au	4.26	7.331	45.56

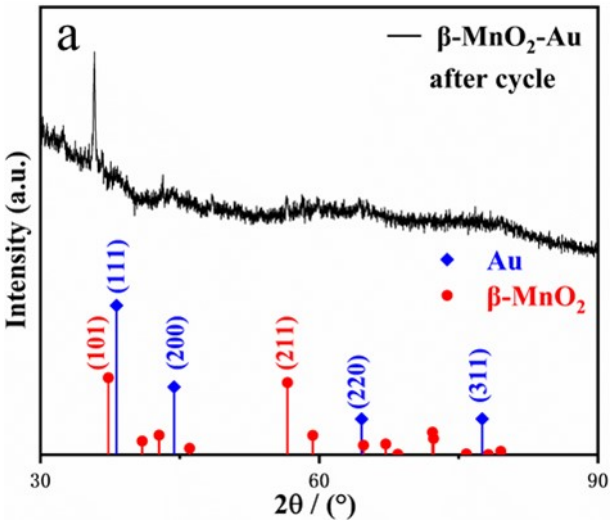

Figure S6 XRD of MnO_2-Au electrode at 60th with a current density of 1 A g^{-1}. Compared with the XRD pattern of initial sample (Fig. S2 (a)), the peak of MnO_2 shifts to lower angle after cycle, which indicates the expanding of MnO_2 (101) plane spacing. The result may come from that lithium ions cannot be completely extracted from MnO_2 during the cycles.

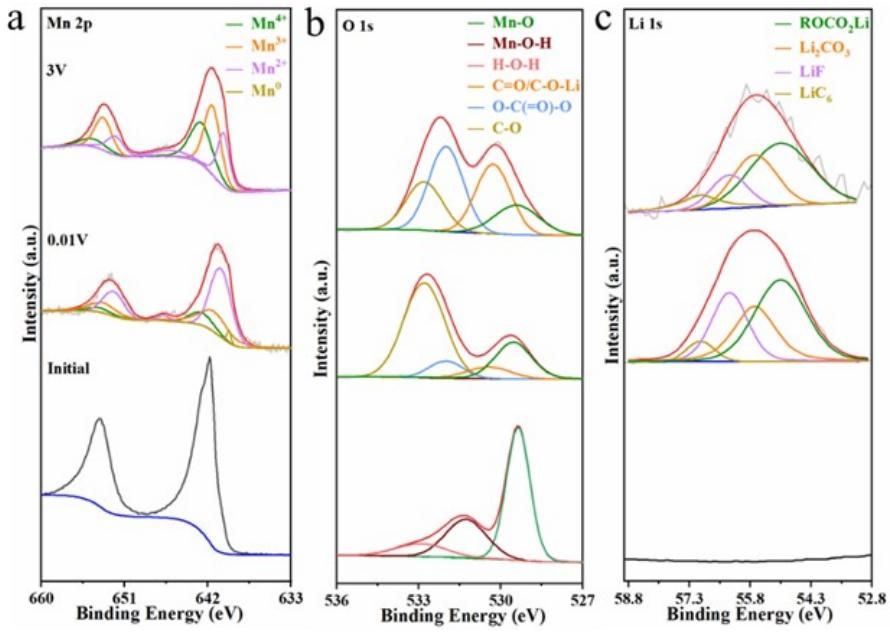

Figure S7. (a) Mn 2p (b) O 1s and (c) Li 1s XPS spectra of MnO_2 electrode at initial, discharge to 0.01 V and charge to 3 V.

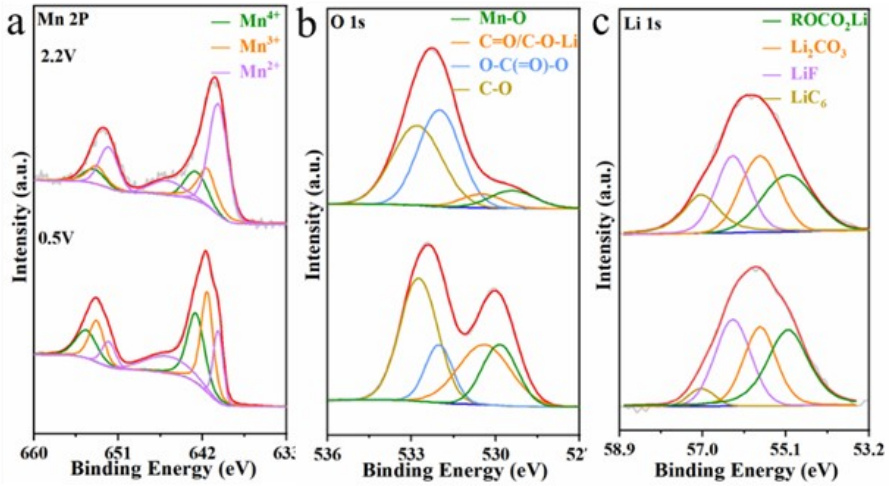

Figure S8. (a) Mn 2p (b) O 1s and (c) Li 1s XPS spectra of MnO_2 electrode at discharge to 0.5 V and charge to 2.2 V.

Table S4 The contents of Au with various valences.

		Au	$Au^{\alpha+}$	$Au^{\beta+}$($\beta > \alpha$)
MnO_2-Au	Initial	100%	0	0
	0.5V	0	41.0%	59.0%
	0.01V	0	100	0
	2.2V	100%	0	0
	3V	100%	0	0

Table S5 The contents of Mn with various valences.

		Mn^{4+}	Mn^{3+}	Mn^{2+}	Mn^{0}
MnO_2-Au	Initial	100%	0	0	0
	0.5V	33.2%	47.8%	13.2%	5.8%
	0.01V	23.5%	6.1%	62.5%	7.9%
	2.2V	26.7%	30.6%	42.7%	0
	3V	40.2%	38.6%	21.2%	0
MnO_2	Initial	100%	0	0	0
	0.5V	39.8%	40.2%	20.0%	0
	0.01V	12.0%	30.0%	55.9%	2.1%
	2.2V	17.7%	25.7%	56.6%	0
	3V	34.3%	40.0%	25.7%	0

Table S6 The content of chemical bond of different oxygen in the initial state of the two materials.

	H-O-H	Mn-O-H	Mn-O-Mn
MnO_2	12.5%	29.0%	58.5%
MnO_2-Au	16.7%	42.3%	41.0%

Table S7 The content of chemical bond of different oxygen.

		Mn-O	C=O/C-O-Li	O-C(=)-O	C-O
MnO_2-Au	0.5V	13.8%	29.9%	23.9%	32.4%
	0.01V	17.4%	14.8%	21.8%	46.0%
	2.2V	8.8%	6.0%	43.6%	41.6%
	3V	8.5%	10.0%	40.6%	40.9%
MnO_2	0.5V	18.5%	27.3%	14.0%	40.2%
	0.01V	22.2%	8.1%	9.0%	60.7%
	2.2V	14.8%	18.5%	30.7%	36.0%
	3V	15.7%	28.8%	34.5%	21.0%

Table S8 The content of chemical bond of different lithium.

		$ROCO_2Li$	Li_2CO_3	LiF	LiC_6
MnO_2-Au	0.5V	18.3%	33.6%	34.1%	14.0%
	0.01V	27.7%	25.1%	24.8%	22.4%
	2.2V	33.3%	25.9%	21.2%	19.6%
	3V	27.4%	40.3%	22.7%	9.6%
MnO_2	0.5V	36.9%	27.9%	30.8%	4.4%
	0.01V	42.7%	26.3%	25.5%	5.5%
	2.2V	30.0%	26.0%	26.6%	17.4%
	3V	46.9%	28.1%	14.9%	10.1%

References

1 N. Zhang, G. Guo, B. He, J. Zhu, J. Wu and J. Qiu, *Journal of Solid State Electrochemistry*, 2020, **24**, 591-599.

2 S. Li, M. Yang, G. He, D. Qi and J. Huang, *Materials (Basel)*, 2021, **14**, 13831-13836.

3 Y. Xu, X. Ye, Y. Qiu, C. Gan, L. Huang, X. Tang and X. Luo, *ChemistrySelect*, 2020, **5**, 13831-13836.

4 C. Chae, K. W. Kim, Y. J. Yun, D. Lee, J. Moon, Y. Choi, S. S. Lee, S. Choi and S. Jeong, *ACS Appl Mater Interfaces*, 2016, **8**, 11499-11506.

5 S.-H. Lee, V. Sridhar, J.-H. Jung, K. Karthikeyan, Y.-S. Lee, R. Mukherjee, N. Koratkar and I.-K. Oh, *ACS Nano*, 2013, **7**, 4242-4251.

6 X. Shen, T. Qian, J. Zhou, N. Xu, T. Yang and C. Yan, *ACS Appl Mater Interfaces*, 2015, **7**, 25298-25305.

7 Y. Liu, S. Sun, J. Han, C. Gao, L. Fan and R. Guo, *Langmuir*, 2021, **37**, 2195-2204.